Available online at www.sciencedirect.com
SCIENCE DIRECT®
Journal of Magnetic Resonance 177 (2005) 236–246
JMR Journal of Magnetic Resonance
www.elsevier.com/locate/jmr

Photo-CIDNP experiments with an optimized presaturation pulse train, gated continuous illumination, and a background-nulling pulse grid

Martin Goez [a,*], K. Hun Mok [b], P.J. Hore [b,*]

[a] Fachbereich Chemie, Martin–Luther-Universität Halle–Wittenberg, Kurt–Mothes-Strasse 2, D-06120 Halle/Saale, Germany
[b] Department of Chemistry, University of Oxford, Physical and Theoretical Chemistry Laboratory, South Parks Road, Oxford OX1 3QZ, UK

Received 22 March 2005; revised 27 May 2005
Available online 8 September 2005

Abstract

Methods to record chemically induced dynamic nuclear polarization (CIDNP) spectra that are virtually free from background magnetization and avoid the sensitivity loss and subtraction artifacts of difference spectroscopy have been developed. Presaturation by a string of composite π/2 pulses, each followed by a defocussing field gradient, is analyzed, and guidelines for the optimization of pulse phases and gradient strengths are derived. Subsequent gated illumination during a grid of π pulses with a prescribed timing causes the background magnetization to vanish at those moments of a pulse sequence when CIDNP magnetization is to be sampled or transferred. By shifting the illumination intervals within such a grid, the sign of the polarizations can be inverted without influencing the development of the background magnetization, allowing a further strong suppression of residual background by a phase cycle. Experimental examples for the application of these methods to more complex CIDNP experiments (1D-CIDNP–COSY, 1D-CIDNP–TOCSY, CIDNP-induced heteronuclear Overhauser effects, water suppression in protein CIDNP) are given.

Keywords: Chemically induced dynamic nuclear polarization; Pulse sequences; Presaturation; Laser methods; Amino acids and proteins

1. Introduction

Measurements of chemically induced dynamic nuclear polarization (CIDNP) [1] are among the most powerful methods for the study of radical reactions. The CIDNP effect is caused by a sorting of the nuclear spins in intermediate radical pairs [2,3], and creates pure z magnetization with a non-Boltzmann distribution (polarization) in the diamagnetic reaction products, which is observed by NMR spectroscopy.

The potential of CIDNP for mechanistic investigations [4] draws on many sources. First, the signs of the polarizations are sensitive to the electron-spin multiplicities of the reacting species, and thus often yield information that is unavailable by other methods. In conjunction with the ease and flexibility with which radical pair generation can be controlled by illumination, with respect to both timing and selectivity, this makes CIDNP particularly valuable for photochemical work. Second, the polarizations establish a precursor–successor relationship between different species on the reaction coordinate because they are generated at an earlier stage than the one in which they are observed. Even more informative, they establish a structural relationship between these species because each polarized nucleus may be regarded as having been labeled with its

* Corresponding authors. Fax: +49 345 5527345 (M. Goez), +44 1865 275410 (P. J. Hore).
E-mail addresses: goez@chemie.uni-halle.de (M. Goez), peter.hore@chem.ox.ac.uk (P.J. Hore).

1090-7807/$ - see front matter © 2005 Elsevier Inc. All rights reserved.
doi:10.1016/j.jmr.2005.06.015

particular polarization at the paramagnetic stage of the reaction. Third, the intermediates can be identified from the polarization pattern (i.e., the relative polarization intensities of the different nuclei in a reaction product) because that pattern represents the frozen EPR spectrum of the radicals.

A pure CIDNP spectrum displays only the NMR signals of polarized nuclei. It might appear that product identification can be severely hampered by the missing signals: The products are typically formed in small amounts only, and increasing the turnover of the reaction to a point where their relaxed NMR spectrum can be recorded might be impracticable, in particular if these products are metastable; besides, experimental results at a high turnover are prone to misinterpretation because of secondary reactions of the products. Fortunately, the whole arsenal of high-resolution NMR can be employed to overcome this limitation. Both coherence transfer methods [5–9] and nuclear Overhauser effects [5–7,10–12] have been applied to systems polarized by CIDNP. In this work, we have additionally combined CIDNP with 1D-TOCSY.

Because a CIDNP experiment is simply the acquisition of a free induction decay during a chemical reaction, all the unreacted molecules of the sample yield their normal NMR signals, which can obliterate the desired CIDNP spectrum despite the signal enhancement by the polarizations because the concentration of reacting molecules is only a small fraction of the bulk concentration. With photo-CIDNP, this can be avoided by a time-resolved experiment [13,14], but only at the expense of a greatly reduced sensitivity. Another way to solve that problem is by recording a spectrum with illumination (i.e., with CIDNP) and subtracting from it a spectrum recorded without illumination (without CIDNP) [15]. Apart from the decrease in the sensitivity by a factor of $\sqrt{2}$, which is due to the fact that the CIDNP signal is acquired once but the noise twice, this method is plagued by the usual artifacts of difference spectroscopy, which are much more severe in this case because the illumination causes the temperature in the first measurement to differ from that in the second.

In this work, we will show how the background problem can be completely eliminated by a presaturation method followed by a pulse sequence that prevents the background from recovering despite prolonged illumination, but allows CIDNP to develop. This approach avoids subtraction artifacts and does not degrade the signal-to-noise ratio. We will demonstrate that it not only permits the acquisition of a normal CIDNP spectrum undisturbed by a background but also retains its favourable properties when it is combined with subsequent coherence or magnetization transfer steps. This building block is thus applicable to practically all types of CIDNP experiments where gated continuous illumination is to be used.

2. Experimental

The CIDNP measurements were carried out on a 600 MHz (14.1 T) Varian INOVA NMR spectrometer with a triple-resonance (^{1}H, ^{13}C, and ^{15}N) 5-mm probe. The light source was a Spectra Physics BeamLok 2080 argon ion laser (multiline mode, 488/514 nm, 10 W output power). Illumination was gated with an NM Laser Products LS200 mechanical shutter (rise and fall times, 0.4 ms) controlled by the spectrometer. The light was brought into the sample by means of an optical fibre, which was inserted into the NMR tube by mounting it into a Wilmad WGS 5BL conical insert [15,16].

All chemicals were obtained in the highest available purity and used as received.

3. Results and discussion

We first describe an optimized presaturation scheme and then the pulse sequence that keeps the background near zero while allowing CIDNP to build up constructively. Finally, we demonstrate the applicability to several variants of CIDNP experiments.

3.1. Presaturation pulse train

It seems natural to apply a sequence ($\pi/2$ pulse—gradient) repetitively to achieve a more complete background suppression than with a single such block. However, care has to be taken to avoid the formation of echoes (the original Hahn echoes and stimulated echoes [17]). In the following, we present an analysis with the aim of obtaining guidelines for the choice of optimum pulse phases and gradient strengths.

Pulse nonidealities are greatly reduced by employing composite pulses; for that reason, we used GROPE-8 pulses [18], e.g., Y$\overline{3}$X4X, throughout. For our calculations, the latter can be replaced to an excellent approximation by the simpler composite pulses obtained by fusing adjacent sub-pulses of opposite phase into a single resultant sub-pulse, i.e., by YX in the example. It is sufficient to restrict the discussion to XY and YX pulses; inclusion of the opposite phases merely leads to sign changes but neither suppresses echoes nor gives rise to additional ones. Likewise, we only take into account sequences where the first composite pulse is XY because starting with the other pulse merely results in a rotation of the coordinate system.

We consider building blocks consisting of one such composite $\pi/2$ pulse followed by a z gradient G_i of strength a_i and duration τ_i. Evolution under J coupling

is negligible because the gradient durations are in the millisecond range. The effect of a building block XYG_i (abbreviated as R_i) is represented by the transformation matrix R_i

$$R_i = \begin{pmatrix} 0 & c_i & s_i \\ 0 & -s_i & c_i \\ 1 & 0 & 0 \end{pmatrix} \tag{1}$$

acting on the product operator basis I_x, I_y, and I_z given as a column vector. The functions

$$c_i = \cos(a_i\tau_i z + \Omega\tau_i), \tag{2}$$

$$s_i = \sin(a_i\tau_i z + \Omega\tau_i), \tag{3}$$

describe the position-dependent precession caused by the field gradient and the position-independent precession under the influence of the chemical shift Ω. For a building block L_j with the pulses in reverse order, YXG_j, one has the matrix L_j,

$$L_j = \begin{pmatrix} s_j & 0 & -c_j \\ c_j & 0 & s_j \\ 0 & -1 & 0 \end{pmatrix}. \tag{4}$$

The action of several blocks in succession is obtained by multiplying the matrices together in reverse order. For example, for R_1 followed by R_2, one gets

$$R_2 \cdot R_1 \cdot \begin{pmatrix} 0 \\ 0 \\ 1 \end{pmatrix} = \begin{pmatrix} c_1c_2 \\ -c_1s_2 \\ s_1 \end{pmatrix}. \tag{5}$$

To gain insight into the dependence of the echoes on the gradient strengths and durations, Eqs. (2) and (3) have to be inserted into Eq. (5) and the products of the trigonometric functions have to be expanded such that their arguments contain either gradient terms or chemical shift terms, but not both. This expansion results in a collection of sine and cosine functions with the sums and differences of the $a_i\tau_i z$ or of the $\Omega\tau_i$ as arguments.

Symmetry can be used to reduce the complexity of the result considerably. Sine functions with gradient arguments are antisymmetric (A) with respect to reflection in the transverse plane passing through the centre of the rf coil, so their integral over the coil region vanishes. The corresponding cosine functions are symmetric (S), and by averaging them over the coil region one obtains sinc functions

$$\frac{1}{l}\int_{-l/2}^{+l/2} \cos(a_i\tau_i z)\mathrm{d}z = \frac{\sin(a_i\tau_i l/2)}{a_i\tau_i l/2} = \mathrm{sinc}(a_i\tau_i l/2). \tag{6}$$

For further simplification, we take all gradient durations to be equal, $\tau_i = \tau$, which will halve the number of terms through its influence on the chemical shift evolution.

Application to Eq. (5) thus yields as the final result

$$R_2 \cdot R_1 \cdot \begin{pmatrix} 0 \\ 0 \\ 1 \end{pmatrix} = \frac{1}{2}\begin{pmatrix} \cos(2\Omega\tau)\mathrm{sinc}[(a_1+a_2)\tau l/2] + \mathrm{sinc}[(a_1-a_2)\tau l/2] \\ -\sin(2\Omega\tau)\mathrm{sinc}[(a_1+a_2)\tau l/2] \\ 2\sin(\Omega\tau)\mathrm{sinc}[a_1\tau l/2] \end{pmatrix}. \tag{7}$$

Echoes arise when the denominator of a sinc function becomes zero or very small, i.e., when the gradient magnitudes are identical or very similar. In the example, an echo would be formed on the x-axis irrespective of the chemical shift, if the gradients had the same signs; if their signs were opposite, the echo would instead be formed along an axis determined by the chemical shift.

In the light of these findings, general guidelines for the choice of the phases of the saturation pulse train can be derived by disregarding chemical shift evolution, i.e., by considering echoes on fixed axes only. For $\Omega = 0$, a train of n groups R–L has a transformation matrix with elements that are either symmetric or antisymmetric

$$(L \cdot R)^n = \begin{pmatrix} S & A & S \\ A & S & A \\ S & A & S \end{pmatrix}. \tag{8}$$

(In the case $n = 1$, the element in the lower left corner is zero.) Adding one block R after n groups of blocks $(R–L)^n$ yields a matrix

$$R \cdot (L \cdot R)^n = \begin{pmatrix} A & S & A \\ S & 0 & S \\ S & A & S \end{pmatrix} \tag{9}$$

the elements of which are again either symmetric or antisymmetric (or zero for the element at the centre). In contrast to this, the elements of the matrix describing a string of nonalternating blocks have mixed symmetries.

Multiplication from the right with the starting condition, pure z magnetization, selects the third column of the matrix Eq. (8) or (9). It is possible to add one final block to the presaturation sequence such that no z magnetization remains by symmetry. For this, the third row of the matrix representing that final block must select an antisymmetric element. It it seen [compare Eqs. (1) and (8), as well as (4) and (9)] that this is the case if the final block of the sequence has the same order of the pulses as the preceding one.

Apart from these two classes of solutions, $(R–L)^n$–L and $(R–L)^n$–R–R, of which R–R (Eq. (7)) is a special case, two others with the same behaviour exist, namely those for which the *first* two blocks are identical and the others alternating. However, the sequences given above have a very desirable property: the symmetry cancellation of the z magnetization also holds for all sequences

that are shortened at the left end. In other words, z magnetization still present after the nth block—caused by pulse imperfections and/or by relaxation—is suppressed in the same manner except that the suppression sequence has fewer blocks.

For more than two blocks, the number of sinc functions entering I_x and I_y rises rapidly. Taking into account that residual z magnetization after the nth pulse experiences a correspondingly shorter sub-sequence, the result comprises all possible combinations of the gradients with all possible sign combinations except for a multiplication of all gradients with -1. For instance, in any three-block sequence one has $(+++)$, $(++-)$, $(+-+)$, $(+--)$, $(0++)$, $(0+-)$, $(+0+)$, $(+0-)$, $(++0)$, and $(+-0)$, when the gradients are always written in the order a_1, a_2, a_3, their sign is represented by $+$ or $-$, and 0 signifies the absence of that gradient in the sinc function.

To eliminate echoes, gradients strengths should, therefore, be chosen such that all the differences formed according to this prescription be nonzero. With regard to their signs, gradients of one polarity are sufficient: As the above example already shows, for each term containing a given gradient with one relative sign there occurs another term that is identical except that that gradient has the opposite relative sign. Experimentally, we obtained very good results with gradient strengths decreasing exponentially, by a factor of typically 0.5–0.7 from block to block. Although inverting the gradient order should leave the differences unchanged, we found that this noticeably deteriorated the results. The most probable reason is that the magnetization to be eliminated is largest at the beginning of the sequence, so it is more efficient if the gradient strengths parallel its decrease.

For $\Omega \neq 0$, the position-independent precession spoils the symmetry cancellation of the z magnetization. However, the effect is only indirect because I_z in an n-block experiment corresponds to the chemical-shift dependent transverse magnetization in an $(n-1)$-block experiment. Hence, both with the sequence R–R (compare Eq. (7)) and with the sequence R–L–L, for which the z magnetization is found to be $\mathrm{sinc}[(a_1+a_2)\,\tau\,l/2]$, no gradient differences enter the sinc functions; this only happens for longer sequences. Pulse nonidealities exert a similar influence. They also introduce sinc terms of gradient differences to I_z but, as can be shown by a first-order treatment, the latter are again fewer in number than for the transverse components in the ideal case; the first of these arises with the sequence R–L–L, and is given by $\mathrm{sinc}[(a_1-a_2)\tau\,l/2]$. It is thus obvious that the same choice of gradients that minimizes echoes will minimize I_z as well.

Fig. 1 displays the improvements obtained by these multiblock sequences. To make the conditions comparable, the sum of all gradient strengths were kept constant throughout. With a single composite $\pi/2$ pulse followed by a gradient, the background suppression did not exceed a factor of 30 although the width of the $\pi/2$ pulse was carefully calibrated. When five such blocks were used, the signals could be further reduced by one order of magnitude. An increase in the number of blocks beyond that did not produce a better suppression. The residual signals are most likely due to pickup from outside the coil region, which cannot be saturated because the flip angle deviates more and more from $\pi/2$ in that

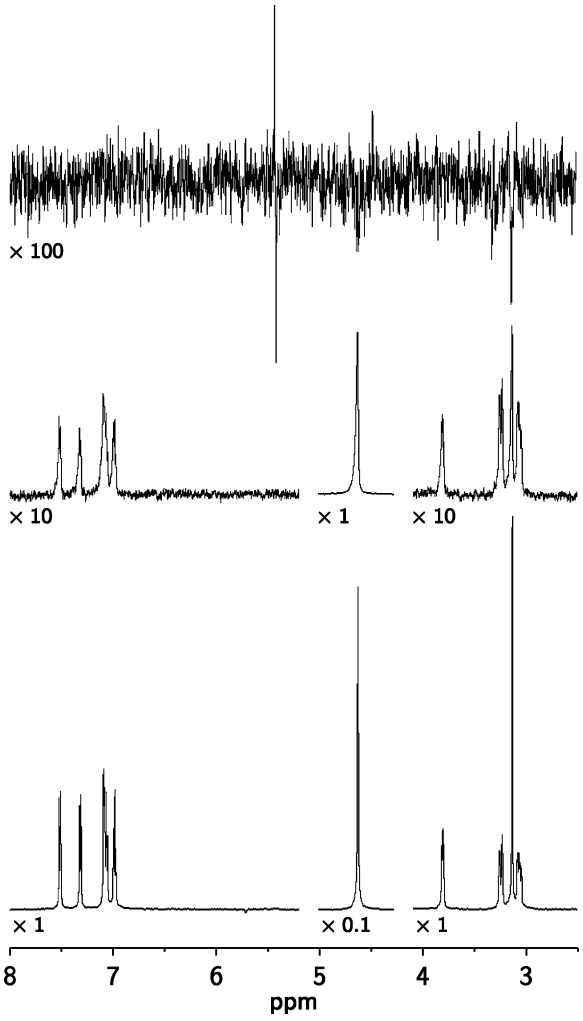

Fig. 1. Background suppression experiments on a sample of 60 mM L-tryptophan in D_2O (HDO peak at 4.6 ppm), pH 7.0, 1 scan each, gradient integral in each experiment $60\ \mathrm{G\,cm^{-1}} \times 5$ ms, residual background read out with a $\pi/2$ pulse after a gradient recovery delay of 5 ms. The signals of the tryptophan α, β, and ring protons (for the structure, see Fig. 6) appear at 3.0–3.3, and 6.0–6.9 ppm, respectively. Scale factors are given below the traces. In the lower two spectra, the water peak was downscaled by a factor of 10. The bottom trace shows the result with one suppression block; compared to the normal NMR spectrum, the signals are already decreased by a factor of about 30. In the centre trace, five blocks with the phase cycle described in the text were used (suppression >300), and in the top trace this was combined with the background-nulling grid and phase cycle of Section 3.2 (suppression >3000). The spikes at 5.5 ppm in the top spectrum are caused by the rf carrier.

range. This is corroborated by the fact that these signals become larger when a $5\pi/2$ pulse is used for sampling. However, a further dramatic improvement of the suppression can be achieved with the illumination sequence described in the next section.

3.2. Background-nulling grid and illumination scheme for CIDNP

Typical illumination times in photo-CIDNP experiments are between a few tens of milliseconds to a few seconds. Even with perfect presaturation, substantial recovery of the background would occur during that time, in particular when the relaxation times T_1 are short (as, e.g., in protein CIDNP).

However, the background is only detrimental at those moments of the pulse sequence, when z magnetization is to be converted into coherence. Some time ago, one of us reported a scheme [19,20] by which the background, after presaturation, is periodically inverted with π pulses such that it oscillates around zero and never fully recovers. When certain timing requirements are met, such a sequence is self-compensating with respect to different relaxation times, i.e., the zero crossings of all the background signals almost coincide regardless of their T_1 values. At these points in time, which form a grid where the background is nulled, pulses with flip angles other than integer multiples of π can be applied without sacrificing the suppression. Outside the field of CIDNP, this scheme has later found use in DPFGSE NOE measurements [21].

Let a single π pulse be preceded by a delay Δ_1 and followed by another delay Δ_2. The timing is chosen such [see below, Eqs. (10)–(12)] that the background of the nucleus with the shortest relaxation time crosses zero at the end of Δ_2. Self-compensation occurs because the other nuclei, which relax more slowly, regain a smaller fraction of their equilibrium magnetization during the pre-pulse period Δ_1, so their relaxation during the post-pulse period Δ_2 starts from a less negative value. The compensation is exact to first order.

Fig. 2 shows the time dependence of the background magnetization for three different relaxation times and complete saturation as the initial condition. In the (realistic) example, the background at the end of Δ_2 does not exceed 0.2% in the worst case, although up to 10% of the background magnetization is recovered before the π pulse. The worst-case error depends only on the ratio $\Delta_1/T_{1,\min}$ (or alternatively, because of the relationships Eq. (10 and 11), on the ratio $\Delta_2/T_{1,\min}$), where $T_{1,\min}$ is the shortest relaxation time of the background [19].

Depending on whether Δ_1 (Eq. (10)), Δ_2 (Eq. (11)), or their sum (Eq. (12)) is constrained by the details of the pulse sequence to be the independent variable, one has to choose

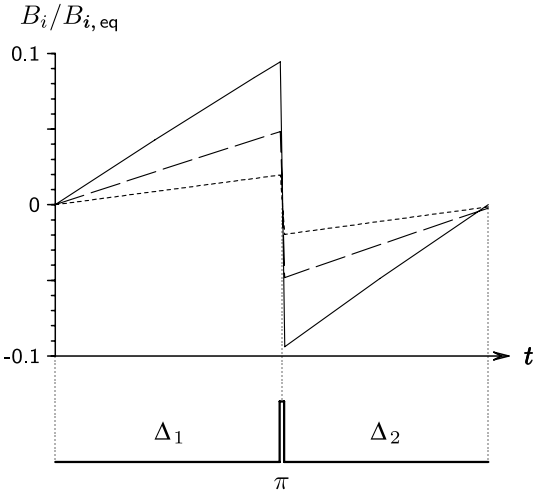

Fig. 2. Development of the background magnetization B_i of nucleus i relative to its equilibrium magnetization $B_{i,\mathrm{eq}}$ during an inversion block as shown below the graph. Solid line, $\Delta_1/T_1 = 0.1$, Δ_2 optimized for this value with Eq. (10); dashed line, $\Delta_1/T_1 = 0.05$; dotted line, $\Delta_1/T_1 = 0.02$. Further explanation, see text.

$$\Delta_2 = T_{1,\min} \cdot \ln[2 - \exp(-\Delta_1/T_{1,\min})], \tag{10}$$

$$\Delta_1 = T_{1,\min} \cdot \ln\left[\frac{1}{2 - \exp(+\Delta_2/T_{1,\min})}\right], \tag{11}$$

$$\Delta_2 = T_{1,\min} \cdot \ln\frac{2}{1 + \exp[-(\Delta_1 + \Delta_2)/T_{1,\min}]}. \tag{12}$$

As is evident from Eq. (11), Δ_2 must not exceed $T_{1,\min} \ln 2$ for the method to be applicable. To fulfil that condition, and because the error decreases when the time slices $\Delta_{1,2}$ become smaller, it is often necessary to use more than one π pulse. In that case, the background magnetization at the start of any block Δ_1–π–Δ_2 after the very first is no longer zero except for the signal with $T_{1,\min}$, for which the timing was optimized. The properties of a sequence of n such blocks have hitherto only been analyzed for odd n [20].

The action of a single block Δ_1–π–Δ_2 is to transform a background signal $B_{i,\mathrm{in}}$ present as its input into an output signal $B_{i,\mathrm{out}}$ according to

$$\begin{aligned} B_{i,\mathrm{out}} &= 1 - (1 - B_{i,\mathrm{in}})\exp[-(\Delta_1 + \Delta_2)/T_{1i}] - 2\exp[-\Delta_2/T_{1i}] \\ &= 1 - (1 - B_{i,\mathrm{in}})\xi - 2\left(\frac{2}{1 + \xi^{T_{1i}/T_{1,\min}}}\right)^{-T_{1,\min}/T_{1i}}, \end{aligned} \tag{13}$$

where T_{1i} is the relaxation time of the signal considered (not necessarily the one, for which the delays were optimized), ξ is an abbreviation for

$$\xi = \exp[-(\Delta_1 + \Delta_2)/T_{1i}] \tag{14}$$

and Eq. (12) was used to express Δ_2 in terms of the variable ξ. For a string of n such blocks and the initial condition of complete presaturation at their beginning, one finds by recursive insertion that the background signal

$B_i(n)$, relative to its equilibrium value $B_{i,\mathrm{eq}}$, after the last block is given by

$$\begin{aligned} B_i(n)/B_{i,\mathrm{eq}} &= \{1+\exp[-(\Delta_1+\Delta_2)/T_{1i}]-2\exp[-\Delta_2/T_{1i}]\} \\ &\quad\times\sum_{j=0}^{n-1}(-1)^j\exp[-j(\Delta_1+\Delta_2)/T_{1i}] \\ &= \left\{1+\xi-2\left(\frac{2}{1+\xi^{T_{1i}/T_{1,\min}}}\right)^{-T_{1,\min}/T_{1i}}\right\} \\ &\quad\times\frac{1-(-\xi)^n}{1+\xi}. \end{aligned} \tag{15}$$

Eq. (15) includes the result for odd n given in [20] as a special case.

The term $[1-(-\xi)^n]/(1+\xi)$ is always positive and smaller than unity; it becomes zero only for infinitely long T_{1i} or infinitely short times $\Delta_{1,2}$. Hence, background nulling is solely governed by the first term of Eq. (15), which is the result for $n=1$. In other words, a string of blocks Δ_1–π–Δ_2 requires the same timing as a single block for optimization of the background suppression, and knowledge or estimation of the shortest relaxation time of the sample is sufficient for this.

Although $[1-(-\xi)^n]/(1+\xi)$ is thus unimportant for the optimization of the delays, it nevertheless exerts a very pronounced and characteristic influence on the background suppression. Fig. 3 illustrates this for the worst-case error with the parameters of Fig. 2. For increasing values of T_{1i}, $[1-(-\xi)^n]/(1+\xi)$ approaches unity if n is odd, and zero if n is even. An even number of blocks is thus generally more favourable than an odd number. The difference becomes very significant for small numbers of blocks: with two blocks, the suppression is higher by an order of magnitude than with one block.

If the pulse sequence to be combined with this background suppression scheme comprises more than one pulse with a flip angle different from π (e.g., the 1D-COSY experiment of the next section), background nulling must

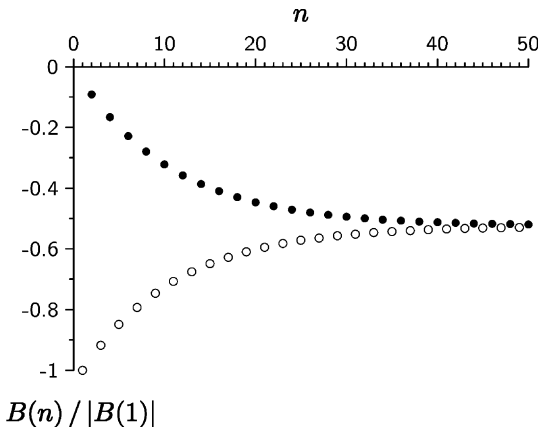

Fig. 3. Residual worst-case background magnetization $B(n)$ with a background-nulling grid of n blocks Δ_1–π–Δ_2 scaled to the absolute value with a single block |B(1)|. Open circles, odd n; filled circles, even n. Further explanation, see text.

be achieved at the moment of each of them. This is always feasible if the sequence allows the insertion of spin echoes in the intervening evolution period. A spin echo demands identical delays around a π pulse, whereas the background suppression scheme demands different delays. Fortunately, these requirements are compatible when *pairs* of spin echoes are employed because the sequence

$$\Delta_1\text{–}\pi\text{–}(\Delta_1+\Delta_2)\text{–}\pi\text{–}\Delta_2 \tag{16}$$

obviously fulfils both. As an additional benefit, the pairwise application of π pulses considerably improves the performance of both spin echoes [22,23] and background nulling (compare Fig. 3). Although the echo delays have to be optimized with the same relationships as before, Eqs. (10)–(12), they are completely independent from the delays during the illumination period.

Because of the periodic inversions, CIDNP would add destructively if the system were illuminated continuously during the train of π pulses. Instead, gated illumination for the duration of one interpulse delay has to be applied following every *second* π pulse. The recognition that this provides another degree of freedom opens up a way of additionally improving the background suppression in quite another way, by a phase cycle (Fig. 4): If an even number of π pulses is used and the gated illumination of alternate slices starts with the very first delay Δ_1, CIDNP from each illumination period experiences an even number of inversion pulses, and thus does not change sign. If the first illumination period follows the first π pulse instead, CIDNP is subjected to an odd number of π pulses, and is thus inverted; the receiver phase has to be adjusted accordingly. However, with respect to the background the situation is absolutely identical in the two cases, so averaging the two transients with the required receiver phase will add CIDNP constructively and the background destructively. The resulting background suppression is virtually complete, as can be seen in Fig. 1.

As shown above, an even number of inversion pulses is conceptually better than an odd number. However, if many pulses are used, the gain is only small, and the added background suppression by the phase cycle might be sufficient. Hence, if other considerations, such as the time required to open or close the shutter, demand that all illuminated slices be of the same length, one can instead use an odd number of π pulses and illuminate only during the slices $\Delta_1+\Delta_2$, as displayed in lower scheme of Fig. 4.

Because the signal experiences, on average, one-half of the π pulses, a high inversion efficiency is mandatory. To ensure that, we used composite pulses (GROPE-16 [24]), which did not lead to any noticeable signal loss in our experiments. A potentially more important drawback of the pulse sequence is that the illumination duty cycle cannot exceed 50%. If the relaxation times are short, this might cause a reduction of the signal. On the other hand, in photo-CIDNP experiments with gated continuous illumination, the number of photons available is rarely a lim-

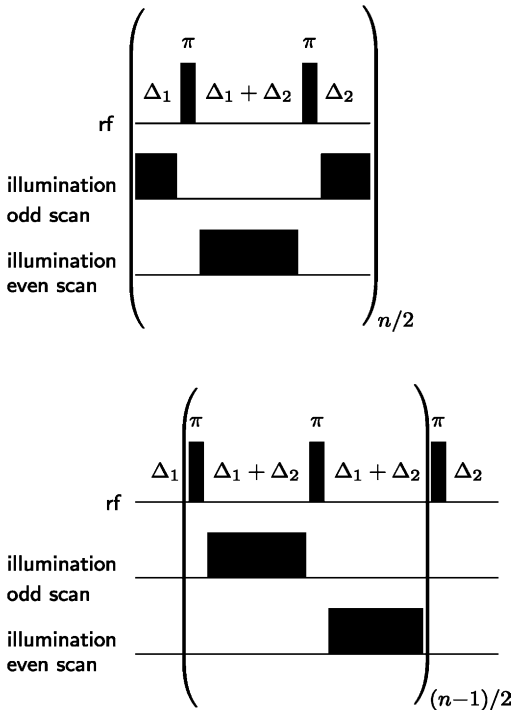

Fig. 4. Background-nulling grid combined with irradiation phase cycle. Upper scheme, for even number n of blocks Δ_1–π–Δ_2; lower scheme, for odd number. The top trace in each figure gives the rf pulse train, the other two traces the illumination scheme for odd-numbered and even-numbered scans. The next element of the pulse sequence, e.g., a hard π/2 pulse, directly follows the final delay Δ_2. The receiver phase is inverted on the even scans. Further explanation, see text.

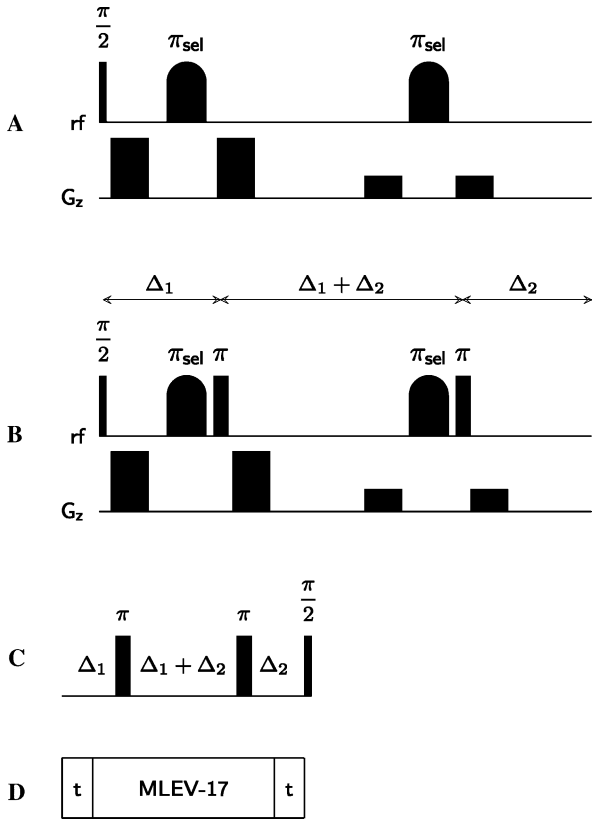

Fig. 5. Building blocks used in the CIDNP experiments, selective excitation (A) and selective suppression (B) by the DPFGSE method [25,26], COSY evolution time (C), and TOCSY mixing sequence (D) [27]. Elements (B)–(D) are followed by an acquisition, whereas element (A) precedes (C) or (D). *Abbreviations:* π_{sel}, selective π pulse; rf, pulse train; G_z, z gradient. The MLEV-17 sequence preceded and followed by a trim pulse t was used for the mixing in the TOCSY sequence [28]. Further explanation, see text.

iting factor, and it is usually feasible to shorten the illumination duration by increasing the laser power.

The described phase cycle might be regarded as a variant of the CIDNP difference spectroscopy normally performed. With it, however, the conditions of the two experiments to be subtracted are much more similar, the only difference being a very slight shift in the illumination timing, so subtraction artifacts due to temperature differences are absent, and there is no noise penalty because there are no alternate dark and light scans, but each scan produces a signal instead. Furthermore, this illumination–suppression sequence can be used as the input to any type of more complex CIDNP experiments, e.g., CIDNP–COSY, because all such experiments are sensitive to the sign of the magnetization initially present.

3.3. Applications

Fig. 5 displays the building blocks other than a simple hard π/2 pulse that were combined with the presaturation and background-nulling schemes in this work.

The first of these (Fig. 5A), selective excitation by the DPFGSE method [25], cannot accommodate nonselective spin echoes that achieve background nulling without sacrificing the selective excitation; the timing requirements of the selective echoes, the nonselective echoes and the background-nulling grid are irreconcilable. However, this does not mean that the background suppression is lost. There is still the phase cycle associated with the illumination scheme, which will strongly suppress any z magnetization recovered during the selective excitation block.

In contrast, for the related selective suppression by the DPFGSE method [26] the timing of the nonselective spin echoes can easily be adjusted such that background nulling is retained (Fig. 5B): Δ_1 is given by the duration of the selective π pulse plus that of the first gradient, which determines Δ_2 (Eq. (10)) and, in turn, the duration of the second gradient. Gradient ringdown delays have to be taken into account. To minimize the total duration of the block, it is advantageous if the first gradient is relatively short and intense.

During the evolution period of a 1D-COSY experiment [27], spin echoes can be applied in pairs (Fig. 5C), and the timing can always be chosen such that background nulling persists. The 1D-TOCSY block of Fig. 5D [27,28] is essentially a train of spin echoes with

extremely short interpulse delays, so it simply freezes any z magnetization present at its start. 1D-NOESY experiments will be discussed in more detail below, because it might be more favourable to perform them with a modification of the illumination scheme. The 2D versions of all these experiments rely on frequency labeling, so the insertion of spin echoes into the evolution period is impossible, and one has to resort to the illumination scheme and phase cycle for background suppression.

Fig. 6, which shows the aromatic part of the NMR and CIDNP spectra of tryptophan with flavin mononucleotide as the photosensitizer, serves to illustrate the use of the blocks of Figs. 5A, C, and D in conjunction with the presaturation and background-nulling grid. By a cyclic reaction, the starting material is regenerated chemically unchanged, but spin-polarized [15]. This system yields strong absorptive polarizations for the ring protons H2, H4, and H6 (for the numbering, see the formula at the top of Fig. 6); H5 and H7 are practically unpolarized. Fig. 6A displays the CIDNP spectrum, which was recorded with the sequence presaturation—illumination grid—$\pi/2$ pulse and the minimum phase cycle of length 2 determined by the illumination scheme. In control experiments without illumination, it was ensured that background suppression is virtually complete in this system (compare Fig. 1, top trace, at a tryptophan concentration 30 times higher). The extremely small absorptive signals of H5 and H7 must, therefore, be a genuine effect.

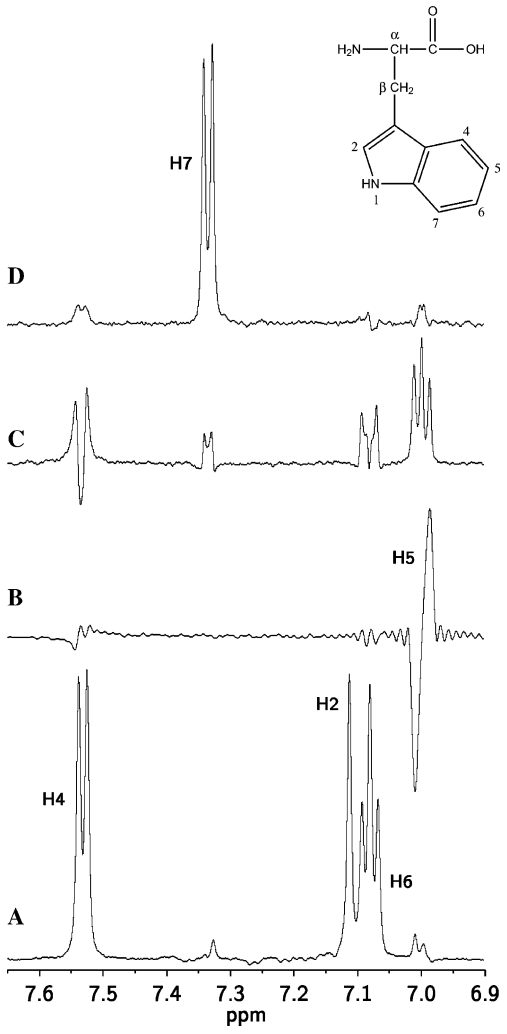

Fig. 6. More complex CIDNP experiments on a sample of 2 mM L-tryptophan and 0.2 mM flavin mononucleotide as the photosensitizer in D_2O, pH 7.0. Shown is the aromatic region of the spectrum. For the assignment of the resonances, see formula at the top. (A) CIDNP spectrum; (B) CIDNP–COSY experiment with selective excitation of H4, pulse sequence, see Figs. 5A and C. Top two traces, CIDNP–TOCSY experiments with 40 ms (C) and 100 ms (D) mixing time, pulse sequence, see Figs. 5A and D. All spectra were recorded with the minimum number of scans determined by the phase cycle and a total illumination duration per scan of 100 ms split into four blocks (see Fig. 4, top); for the calculations of Δ_1 and Δ_2 with Eqs. (11) and (12), $T_{1,\min}$ was set to 2 s. Further explanation, see text.

The virtual absence of these signals highlights a potential difficulty of CIDNP. For an unknown product, it might have been impossible to deduce the topology of the spin system on the basis of such a spectrum only; in particular, the missing signals of the coupling partners of H2 and H4 would have made it impossible to decide whether each observed signal were due to a single proton or several. However, coherence transfer experiments provide all this information. H4 is sufficiently separated from the other polarized signals to allow selective excitation, and a 1D-COSY experiment (Fig. 6B) immediately reveals the signal of H5 in antiphase. Presaturation and illumination were followed by the two building blocks of Figs. 5A and C. Inverting the first pulse yields the minimum phase cycle of a 1D-COSY experiment [27]; by combining this with the phase cycle of the illumination scheme, one arrives at a minimum phase cycle of length 4 for the 1D-CIDNP–COSY experiment.

The connectivity beyond H5 can be explored by the stepwise addition of more coherence transfer steps, but a much more rational way of doing this is by a 1D-TOCSY sequence [27]. For the combination of presaturation and illumination blocks with the sequences of Figs. 5A and D, we again used the minimum phase cycle (length 2 for the 1D-TOCSY experiment times length 2 for the illumination scheme). With increasing mixing time, the signals in a TOCSY experiment travel further away from their source along a J-coupled chain, and also show some oscillatory behaviour. This can be nicely seen in the two top traces of Fig. 6. For a mixing time of 40 ms (C), the signals of H5, H6, and H7 appear with decreasing intensities, and a mixing time of 100 ms (D) yields only the signal of the most remote—and unpolarized—proton H7. Although the product was known in this case, the significance for mechanistic studies by CIDNP is evident.

In the homonuclear case, nuclear Overhauser effects from polarized nuclei to others can be measured in a

very similar way as in the described 1D-CIDNP–COSY or 1D-CIDNP–TOCSY experiments. One simply has to replace the mixing sequence of Figs. 5C or D by a sequence composed of a hard $\pi/2$ pulse for flipping the selectively excited coherence back to the positive or negative z axis, a string of hard π pulses to retain the background suppression during mixing, and a hard readout pulse [21]. Alternatively, because the polarized signals are only a small subset of the NMR spectrum, especially in a protein, it might be of interest just to determine whether there are any cross polarizations at all, regardless of their source. This can be done by either of two strategies: The illumination duration can be increased—which is possible with the described background-nulling grid without sacrificing the background suppression, but might introduce effects due to secondary photochemistry—or the illumination can be stopped some time before the end of the background-nulling grid so as to use the remaining time for mixing without CIDNP generation, i.e., a grid with illumination can be followed by another without illumination.

Overhauser effects from polarized heteronuclei to protons might be even more valuable, because they reduce the complexity of a crowded spectrum even further. In that case, the background-nulling grid is potentially capable of yielding a higher sensitivity. This stems from the recognition that the relaxation times of biologically relevant heteronuclei, in particular ^{15}N, are much longer than T_1 times of protons, so heteronuclear CIDNP can build up over several acquisitions of proton signals and reach much higher values, if precautions are taken that this accumulation is not spoiled.

To that end, we devised the pulse sequence displayed in Fig. 7. It draws on the idea that the z magnetization of the heteronucleus is inverted on every second scan, which inverts the sign of the Overhauser effect, and that the receiver phase is inverted in parallel, so all proton signals except those caused by cross relaxation are cancelled, and the Overhauser effects are added constructively. However, after a scan where the heteronucleus was inverted, one either has to destroy its magnetization or apply an additional inversion pulse because otherwise CIDNP from the preceding scan and newly generated CIDNP would have opposite signs. With the second method, we observed annoying coherence transfer artifacts in our systems because the situation is not identical with respect to the background. However, by interleaving the phase cycle of the illumination scheme and the periodic inversion of the heteronucleus, a phase cycle of length 4 can be constructed that both utilizes the heteronuclear CIDNP to the full extent and is free from the artifacts. The possibility to invert the sign of the polarizations by the illumination grid provides the additional degree of freedom to achieve constructive addition of the heteronuclear CIDNP, and both scans with and scans without the first inversion pulse on the heteronucleus occur in pairs that are subtracted by the receiver phase. Hence, cancellation is not effected by subtraction of scans with and without that pulse, resulting in a virtual absence of coherence transfer artifacts.

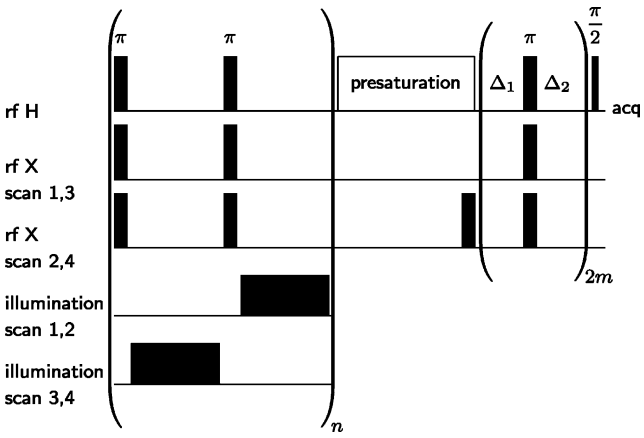

Fig. 7. Application of the illumination scheme and the background-nulling grid to heteronuclear Overhauser effects from X to H. Illumination is not done on a saturated state, so the interpulse delays have not been specified in the illumination grid. Presaturation, with the method described in Section 3.1, is only done for H, and after the illumination. The evolution period for the Overhauser effects is a background-nulling grid for H with an even number of inversions. Further explanation, see text.

^{15}N labeled tryptophan, again with flavin mononucleotide as the photosensitizer, provides an example (Fig. 8). Owing to the unfavourable gyromagnetic ratio γ of the heteronucleus, the signal-to-noise ratio is low, but the spectrum clearly shows the signals of H2 in the aromatic ring and HDO. The latter signal must be due to chemical exchange [10] of the protons at the indole nitrogen because in control experiments of the background suppression no HDO signal was visible under the same conditions. It is also not very surprising because the distance between the indole nitrogen and its directly bound proton is about one-half of the distance between that nitrogen and H2, which shows appreciable cross polarization. Taking into account the r^{-6} distance dependence of the nuclear Overhauser effect and the degree of deuteration of the solvent to estimate the H/D ratio on the indole nitrogen, one would expect an Overhauser effect of that magnitude.

Direct observation of ^{15}N CIDNP shows that the indole nitrogen is strongly polarized in emission [9]. Because of the negative γ of ^{15}N, a proton signal resulting from cross polarization has the same sign as the nitrogen z magnetization. Repeating the experiment of Fig. 8 in a manner suitable for observing nuclear Overhauser effects without CIDNP led to an inversion of the signals (and also gave an Overhauser effect for the α proton, which is unobservable in the experiment of Fig. 8 because the amino nitrogen is unpolarized), which corroborates that they are induced by cross relaxation from the negatively polarized indole nitrogen.

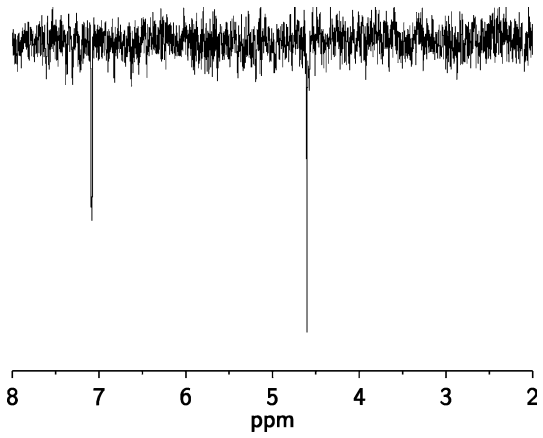

Fig. 8. Chemically induced nuclear Overhauser effect from ^{15}N to ^{1}H in a sample of 2 mM ^{15}N labeled L-tryptophan and 0.2 mM flavin mononucleotide as the photosensitizer in D_2O, pH 7.0. The signals of H2 (compare the formula at the top of Fig. 6) at 7.1 ppm and of HDO (because of exchange with the proton at the indole nitrogen) at 4.6 ppm appear in emission. Pulse sequence, see Fig. 7; total illumination duration per scan, 100 ms; NOE mixing time, 4 s; other parameters, $n = 1$, $2m = 16$. For the calculations of Δ_1 and Δ_2 with Eqs. (11) and (12), $T_{1,min}$ was set to 2 s. Further explanation, see text.

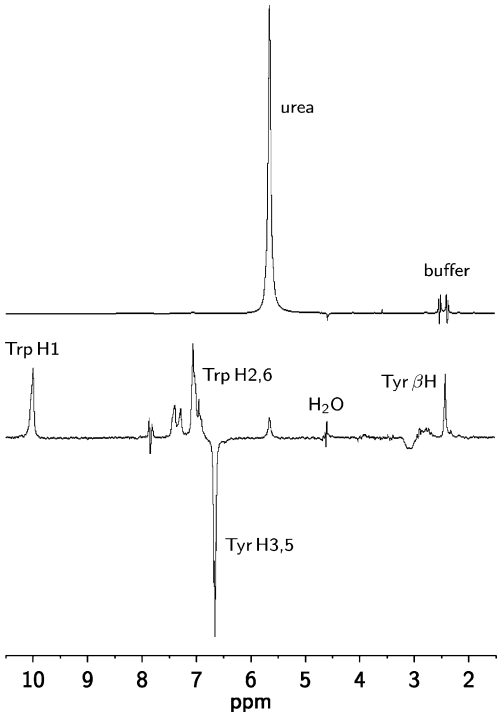

Fig. 9. CIDNP of 1.7 mM bovine α-lactalbumin and 0.2 mM flavin mononucleotide as photosensitizer in 90:10 H_2O/D_2O (4.6 ppm), 50 mM sodium citrate buffer (2.4–2.6 ppm, signals slightly distorted by the DPFGSE sequence), and with 6 M urea (5.67 ppm) added as denaturant. Top trace, spectrum without illumination recorded with the DPFGSE solvent suppression sequence of Fig. 5B. Bottom trace, CIDNP spectrum, pulse sequence presaturation—illumination—DPFGSE suppression. Total illumination duration per scan, 50 ms split into five blocks (see Fig. 4, bottom). For the calculations of Δ_1 and Δ_2 with Eqs. (11) and (12), a value of 300 ms was used for $T_{1,min}$. Further explanation, see text.

Coherence transfer artifacts are seen to be completely absent.

Finally, a protein CIDNP spectrum (bovine α-lactalbumin photosensitized by flavin mononucleotide, Fig. 9) serves to illustrate another potential advantage of the pulse sequences of this work. Proteins often have to be measured in H_2O instead of D_2O, causing a huge z magnetization to be present. While the presaturation and background-nulling sequence are capable of suppressing most of that signal, slightly better results are obtained when the DPFGSE solvent suppression scheme [26] of Fig. 5B is combined with it, as was done in the experiment of Fig. 9.

The solution was buffered by sodium citrate and a high concentration of urea was added as a denaturant. The top trace of Fig. 9 displays the dark spectrum. When the water peak is eliminated by the DPFGSE water suppression scheme, the spectrum is dominated by the signals of the denaturant and buffer. In the CIDNP spectrum (bottom trace), however, the situation is totally different. Not only is the water signal reduced to a level that is much lower than the polarizations but also the urea signal, despite the disparity in the concentrations of protein and denaturant by more than three orders of magnitude; the buffer signal is completely suppressed. While it would be possible to design a shaped pulse that simultaneously eliminates all three signals with the DPFGSE method, this would also render unobservable all CIDNP signals hidden below any of them because that suppression technique relies on elimination of a certain frequency range from the spectrum. In contrast, the presaturation and background-nulling method of this work operates by elimination of z magnetization according to its source, equilibrium magnetization or CIDNP, so observation of CIDNP is also possible in spectral ranges where background signals would appear if unsuppressed. As can be seen, this is the case at 2.45 ppm where an absorptive polarization, due to the tyrosine β protons in this denatured protein [29], become visible when the buffer signals are suppressed.

4. Conclusions

We envision the techniques reported in this paper to have their greatest potential in the field [11,15] of protein CIDNP. They are well suited to suppressing background signals with short T_1 times, which are typical for proteins. Even more promising is their application to folding studies, which are often carried out with high concentrations of denaturants and may exhibit severe subtraction artifacts with the conventional difference spectroscopy approach. For instance, the residual proton signals of the frequently employed denaturant guanidine deuterochlo-

ride (6.70 ppm) fall in the region of the aromatic tyrosine CIDNP signals, the presence of which would furnish proof of the surface accessibility of these residues. An efficient background suppression scheme as described here will permit the observation of polarizations with low intensities in that region, which may be of importance for probing the folding mechanism.

Acknowledgments

Financial support from the BBSRC and INTAS (Project No. 02-2126) and the DFG (Grants Go615/6-3 and Go615/9-1) is gratefully acknowledged. K.H.M. was funded by a Chevening Scholarship (UK Foreign and Commonwealth Office), the OCMS, and the BBSRC. We thank Lars Kuhn and Ilya Kuprov for helpful discussions.

References

[1] J. Bargon, H. Fischer, U. Johnsen, Nuclear magnetic resonance emission lines during fast radical reactions. I. Recording methods and examples, Z. Naturforsch. A 22 (1967) 1551–1555.
[2] G.L. Closs, Mechanism explaining nuclear spin polarizations in radical combination reactions, J. Am. Chem. Soc. 91 (1969) 4552–4554.
[3] R. Kaptein, L.J. Oosterhoff, Chemically induced dynamic nuclear polarization. II. Relation with anomalous ESR spectra, Chem. Phys. Lett. 4 (1969) 195–197.
[4] See, e.g., M. Goez, Photochemically induced dynamic nuclear polarization, in: D.C. Neckers, D.H. Volman, G. von Bünau (Eds.), Advances in Photochemistry, vol. 23, Wiley, New York, 1997, pp. 63–164, and references therein.
[5] R.M. Scheek, S. Stob, R. Boelens, K. Dijkstra, R. Kaptein, Applications of two-dimensional proton nuclear magnetic resonance methods in photochemically induced dynamic nuclear polarization spectroscopy, J. Chem. Soc. Faraday Disc. 78 (1984) 245–256.
[6] R.M. Scheek, S. Stob, R. Boelens, K. Dijkstra, R. Kaptein, Applications of two-dimensional NMR methods in photochemically induced dynamic nuclear polarization spectroscopy, J. Am. Chem. Soc. 107 (1985) 705–706.
[7] S. Stob, R.M. Scheek, R. Boelens, K. Dijkstra, R. Kaptein, Applications of two-dimensional proton NMR methods to photochemically induced dynamic nuclear polarization spectroscopy, Isr. J. Chem. 28 (1989) 319–327.
[8] M. Goez, Coherence transfer by selective pulses in photo-CIDNP experiments, J. Magn. Reson. A 102 (1993) 144–150.
[9] C.E. Lyon, J.A. Jones, C. Redfield, C.M. Dobson, P.J. Hore, Two-dimensional ^{15}N–^{1}H photo-CIDNP as a surface probe of native and partially structured proteins, J. Am. Chem. Soc. 121 (1999) 6505–6506.
[10] J. Bargon, G.P. Gardini, Transfer of CIDNP via proton exchange and nuclear Overhauser effect, J. Am. Chem. Soc. 101 (1979) 7732–7733.
[11] P.J. Hore, R.W. Broadhurst, Prog. Nucl. Magn. Reson. Spectrosc. 25 (1993) 345–402, and references therein.
[12] I. Kuprov, P.J. Hore, Chemically amplified ^{19}F–^{1}H nuclear Overhauser effects, J. Magn. Reson. 168 (2004) 1–7.
[13] S. Schäublin, A. Wokaun, R.R. Ernst, Pulse techniques applied to chemically induced dynamic nuclear polarization, J. Magn. Reson. 27 (1977) 273–302.
[14] G.L. Closs, R.J. Miller, Laser flash photolysis with NMR detection. Microsecond time-resolved CIDNP: separation of geminate and random-phase processes, J. Am. Chem. Soc. 101 (1979) 1639–1641.
[15] K.H. Mok, P.J. Hore, Photo-CIDNP methods for studying protein folding, Methods 34 (2004) 75–87, and references therein.
[16] J.E. Scheffler, C.E. Cottrell, L.J. Berliner, An inexpensive, versatile sample illuminator for photo-CIDNP on any NMR spectrometer, J. Magn. Reson. 63 (1985) 199–201.
[17] E.L. Hahn, Spin echoes, Phys. Rev. 80 (1950) 580–594.
[18] A.J. Shaka, C. Bauer, R. Freeman, Selective population transfer effects in nuclear Overhauser experiments, J. Magn. Reson. 60 (1984) 479–485.
[19] M. Goez, Pseudo steady-state photo-CIDNP measurements, Chem. Phys. Lett. 188 (1992) 451–456.
[20] M. Goez, Pseudo steady-state photo-CIDNP measurements with improved background suppression, Appl. Magn. Reson. 5 (1993) 113–126.
[21] K. Stott, J. Keeler, Q.N. Van, A.J. Shaka, One-dimensional NOE experiments using pulsed field gradients, J. Magn. Reson. 125 (1997) 302–324.
[22] H.Y. Carr, E.M. Purcell, Effects of diffusion on free precession in nuclear magnetic resonance experiments, Phys. Rev. 94 (1954) 630–638.
[23] S. Meiboom, D. Gill, Modified spin-echo method for measuring nuclear relaxation times, Rev. Sci. Instrum. 29 (1958) 93–102.
[24] A.J. Shaka, R. Freeman, Composite pulses with dual compensation, J. Magn. Reson. 55 (1983) 487–493.
[25] K. Stott, J. Stonehouse, J. Keeler, T.-L. Hwang, A.J. Shaka, Excitation sculpting in high-resolution nuclear magnetic resonance spectroscopy: application to selective NOE experiments, J. Am. Chem. Soc. 117 (1995) 4199–4200.
[26] T.-L. Hwang, A.J. Shaka, Water suppression that works. Excitation sculpting using arbitrary waveforms and pulsed field gradients, J. Magn. Reson. A 112 (1995) 275–279.
[27] H. Kessler, H. Oschkinat, C. Griesinger, W. Bermel, Transformation of homonuclear two-dimensional NMR techniques into one-dimensional techniques using Gaussian pulses, J. Magn. Reson. 70 (1986) 106–133.
[28] A. Bax, D.G. Davis, MLEV-17-based two-dimensional homonuclear magnetization transfer spectroscopy, J. Magn. Reson. 65 (1985) 355–360.
[29] K. Maeda, C.E. Lyon, J.J. Lopez, M. Cemazar, C.M. Dobson, P.J. Hore, Improved photo-CIDNP methods for studying protein structure and folding, J. Biomol. NMR 16 (2000) 235–244.